Heat transfer enhancement by a focused ultrasound field

Journal Article

Author(s):
Wang, Xiaowu; Wan, Zhenping; Chen, Boqian; Zhao, Yongling

Heat transfer enhancement by a focused ultrasound field

Xiaowu Wang, Zhenping Wan 🄳 , Boqian Chen, and Yongling Zhao 🄳

View Online   Export Citation   CrossMark

ARTICLES YOU MAY BE INTERESTED IN

Heat transfer enhancement by a focused ultrasound field

View Online   Export Citation   CrossMark

Xiaowu Wang,[1] Zhenping Wan,[2,a] (iD) Boqian Chen,[2] and Yongling Zhao[3] (iD)

AFFILIATIONS

[1] Department of Physics, School of Science, South China University of Technology, Guangzhou 510640, China
[2] School of Mechanical and Automotive Engineering, South China University of Technology, Guangzhou 510640, China
[3] Department of Mechanical and Process Engineering, ETH Zürich, Zürich 8093, Switzerland

[a] Author to whom correspondence should be addressed: zhpwan@scut.edu.cn

ABSTRACT

A focused ultrasound field is set up in a heat transfer cavity with an elliptical cross section. A sound source and a heat source are designed at the two focus points where the sound intensity is reinforced based on the interference and standing wave criteria. The sound intensities and heat transfer coefficients of the cavity with a focused ultrasonic field and an ordinary cavity with a rectangular cross section are measured under the natural convection heat transfer regime. The distribution of the heat transfer coefficient matches the distribution of the sound intensity. The heat transfer performance is then enhanced in the cavity with a focused ultrasonic field. The cavitations and acoustic streaming characteristics in the cavity with a focused ultrasonic field and the ordinary cavity are also studied. The velocity of acoustic streaming is larger in the cavity with a focused ultrasonic field than in the ordinary cavity, and no cavitation is observed in the ordinary cavity. Although the cavitation cloud around the heat source is unfavorable for the heat transfer in the cavity with a focused ultrasonic field, the cavitations collapse and the resulting high temperature, higher pressure, and microjet effects still contribute substantially to heat transfer.

I. INTRODUCTION

The ability of ultrasonic waves to be used for heat transfer enhancement has been known since the 1960s.[1–3] Tam *et al.*[4] studied the influence of ultrasound on the heat transfer inside horizontal tubes in the laminar region. Their results showed that a substantial heat transfer enhancement via ultrasound is observed and that two ultrasonic heads can give a better heat transfer enhancement in the entrance and in fully developed regions. Chen *et al.*[5] studied the enhancement of the heat transfer performance under ultrasonic vibration. They then reported that the maximum heat transfer increment can be up to 1557 W/(m^2 K) and that the maximum heat transfer increment ratio can be ~301%. They also presented empirical correlations for heat transfer enhancement under ultrasonic vibration. Baffigi and Bartoli[6] experimentally investigated the influence of ultrasonic waves on the heat transfer enhancement under sub-cooled boiling conditions. They declared that ultrasonic waves seem to be quite useful for practical applications in cooling electronic components. It is believed that the heat transfer enhancement with

ultrasound is due to the physical effects induced by cavitations and acoustic streaming. Liu *et al.*[7] studied the motion and the dynamical characteristics of a single cavitation bubble between two parallel plates on the heat transfer. They found that the bubble between two parallel walls is at first split into two smaller sub-bubbles; then, these sub-bubbles further collapse near the upper and lower walls. The second collapse of the sub-bubbles has a greater impact on the heat transfer than the first collapse. Orandrou *et al.*[8] studied the influence of acoustic streaming on single-phase heat transfer through simulations and experiments. They simulated the flow field distribution under the combined action of acoustic streaming and thermal convection and tested the actual velocity field by using a particle image velocimeter. Their results showed that the influence of acoustic streaming on single-phase heat transfer is not obvious and that the enhancement rate is 5%. Zheng *et al.*[9] investigated the ultrasonic heat transfer enhancement on three different structural tubes (smooth, screwed, and finned) in an LiBr solution in the sub-cooled boiling regime. The influences of the ultrasound parameters (e.g., frequency and power) on the sub-cooled boiling heat transfer of

the three different structural tubes were investigated, and the sound pressure distribution around the tested tubes was used to describe the mechanism of the ultrasonic heat transfer enhancement. Baffigi and Bartoli[10] found that ultrasound will decrease the heat transfer coefficient of saturated boiling because no ultrasonic cavitations can be generated. However, ultrasound can delay the transition from nucleate boiling to film-style boiling.

Other ultrasound-related factors that influence the ultrasonic heat transfer enhancement have also been studied. Zhao et al.[11] studied the influence of ultrasound on bubble nucleation and the heat transfer enhancement of nanofluids. They found that nanoparticles can enhance the bubble nucleation and ultrasound can enhance the bubble oscillating motion in an interconnected capillary loop. Mathur et al.[12] studied the difference in the heat transfer enhancement between high frequency ultrasound and low frequency ultrasound. They reported that high-frequency ultrasound can produce more ultrasonic cavitations and stronger microacoustic flow is generated by cavitations. Bubble flow is the main reason for enhancing heat transfer. They also studied the influence of the number of applied ultrasonic transducers on the heat transfer enhancement. Their results showed that the ultrasonic enhancement rate will decrease if two or more transducers are used at the same time. Bartoli et al.[13] investigated the influence of the ultrasound on the heat transfer rate in the sub-cooled boiling regime. They studied the influences of the water sub-cooling degree, the ultrasonic generator power, and the heat flux on the heat transfer performance. They believed that ultrasonic waves can induce turbulence. Xia and Sun[14] reported an acoustic focusing effect through a simple brass circular ring structure immersed in water. They found that the acoustic waves can be well focused on the center of the ring and the focusing effect is closely related to the size and shape of the ring structure. Xia et al.[15] also reported a multifocal acoustic focusing lens using a simple metal cylinder structure immersed in water. They realized one or more focus points by the excited Mie-resonance modes in the cylinder structure. Hong and Kim[16] derived the general solution of the wave equation in elliptic co-ordinates and then obtained the period or pulsatance equation by substituting the solution of the wave equation into the boundary condition. The authors numerically calculated natural frequencies and mode shapes of elliptical, cylindrical, and annular cylinder acoustic cavities, which have the same cross-sectional area and volume. They also discussed the influence of the eccentricity on the general characteristics of cylindrically shaped acoustic devices. Their reports can be used to conduct modal analysis numerically or perhaps semi-analytically.

It is accepted that the benefit of ultrasonic heat transfer enhancement mainly comes from ultrasonic cavitations and acoustic streaming, which are all related to the sound intensity near the heat transfer surface. The higher the local sound intensity, the stronger the cavitations' effect, the higher the acoustic streaming velocity, and, therefore, the better the heat transfer performance. However, until now, most of the conducted research was focused on the influences of the heat transfer surface structure, ultrasonic power, ultrasonic frequency, and location of the sound source. There is little particular study on how the sound intensity distribution affects the ultrasonic heat transfer enhancement. In this paper, ultrasonic wave interference enhancement and the standing wave phenomena are constructed in a cavity in order to obtain the strengthened local sound intensity around the heat source. The characteristics of the cavitations and acoustic streaming around the heat source are studied experimentally to find the effect of the sound intensity on the ultrasonic heat transfer enhancement.

II. THE DESIGN OF THE CAVITIES

In order to keep the sound intensity around the heat source always stronger, the propagation process of the acoustic wave in the cavity should be stable and periodic. That is necessary to form a standing wave in the cavity. Figure 1 shows the simulated focusing process of a single pulse ultrasonic wave in an ellipse with the aid of finite element solver COMSOL Multiphysics. The ultrasound is considered to be a wave with small amplitude. The ultrasonic pressure satisfies the following equation:

$$\frac{1}{\rho c_0^2}\frac{\partial^2 p}{\partial t^2} = \frac{1}{\rho}\nabla^2 p + \frac{b}{\rho^2 c_0^2}\nabla^2\frac{\partial p}{\partial t} + \frac{dg}{dt}\delta^{(2)}(\vec{r}-\vec{r}_0). \quad (1)$$

If the medium is viscous, it will absorb the acoustic wave. The heat transfer from the compression zone to the expansion zone also involves acoustic energy dissipation. The last term on the right-hand side of Eq. (1) corresponds to the influence of viscous force and the heat transfer on wave propagating. The viscous force per unit area is proportional to the gradient of the velocity. The proportionality coefficient includes two parts: one is $\frac{4}{3}\eta'$ and the other is η''. The term $\kappa_t\left(\frac{1}{C_v}-\frac{1}{C_p}\right)$ is the influence owing to the heat transfer. Hence, parameter b satisfies

$$b = \frac{4}{3}\eta' + \eta'' + \kappa_t\left(\frac{1}{C_v}-\frac{1}{C_p}\right). \quad (2)$$

$\delta^{(2)}$ the is Dirac function, $\vec{r}$ is the position of the field point, and $\vec{r}_0$ is the position of the sound source. g is a single Gaussian pulse at the left focus point, which is defined as

$$g = \begin{cases} Ae^{-\pi^2 f_0^2(t-t_p)^2}, & 0 \le t \le 2t_p \\ 0, & t > 2t_p. \end{cases}$$

Boundary condition: $\frac{\partial p}{\partial \vec{n}} = 0$ on all walls.

Initial condition: $p = 0$,

$$\frac{dp}{dt} = 0.$$

Here, p and ρ are the ultrasonic pressure and the equilibrium density of the working fluid, respectively, t is the time, c_0 is the ultrasonic velocity, v is the velocity, and C_v and C_p are the isometric heat capacity and isobaric heat capacity, respectively. η' and η'' are the shear viscosity coefficient and bulk viscosity coefficient, respectively. κ_t is the thermal conductivity of the medium. g represents a single Gaussian pulse. A and p_0 are the amplitude of the single Gaussian pulse (4 m² s⁻¹ here) and the pressure in the cavity without acoustic perturbation, respectively. Symbol t_p is the time to peak and is 5×10^{-6} s in this manuscript. T is the temperature. f_0 is the reciprocal of t_p.
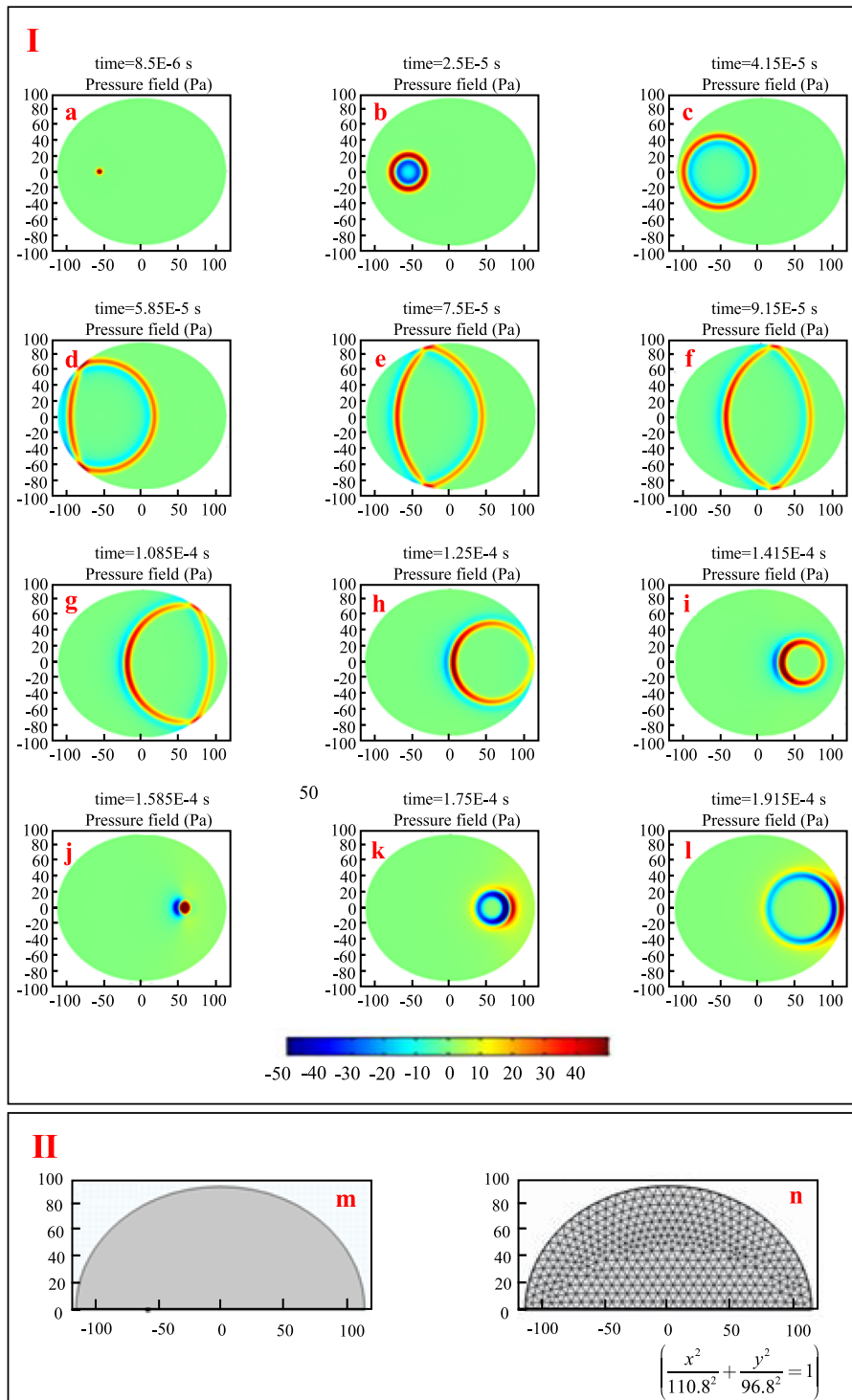
FIG. 1. The focusing process of a pulsed ultrasonic wave. The focusing process of a pulsed ultrasonic wave at (a) time = 8.5 × 10^{-6} s; (b) time = 2.5 × 10^{-5} s; (c) time = 4.15 × 10^{-5} s; (d) time = 5.85 × 10^{-5} s; (e) time = 7.5 × 10^{-5} s; (f) time = 9.15 × 10^{-5} s; (g) time = 1.085 × 10^{-4} s; (h) time = 1.25 × 10^{-4} s; (i) time = 1.415 × 10^{-4} s; (j) time = 1.585 × 10^{-4} s; (k) time = 1.75 × 10^{-4} s; and (l) time = 1.915 × 10^{-4} s; (m) the geometric model and (n) the mesh.

$$\left(\frac{x^2}{110.8^2} + \frac{y^2}{96.8^2} = 1\right)$$

In the simulation, the application mode of transient sound pressure in the acoustic module of COMSOL Multiphysics is adopted. The working fluid is water at temperature 40 °C. The left focus of the ellipse is set as a wave source point, and the wave is a single Gaussian pulse sound wave emitted by the wave source. It has wavelength 55.4 mm and wave velocity 1550.0 m/s. In order to reduce the calculation amount of the model, the axisymmetric method is used. The symmetry axis is set as an acoustic hard

boundary, and only the wave equation formulated in one half of the ellipse is solved. Then, the whole results are displayed through the function of the "two-dimensional image." The ellipse equation and mesh of the model in the simulation are shown in Figs. 1(m) and 1(n). A triangular mesh is used here. When choosing the solver, the defaulted values are saved. An adaptive mesh is chosen. The time step is 0.5×10^{-6} s. After the mesh independence verification, the maximum and the minimum cell sizes of the grid are 8.2 mm and 0.3 mm, respectively.

As seen from Fig. 1, the evolution of the pulse ultrasonic wave is periodic and symmetrical along the long axis of the ellipse. The wave front of the single pulse sound wave emitted from the sound source located at the left focus of the ellipse forms an annular acoustic wave front. Then, the left half of the annular acoustic wave front is reflected and forms a spindle-shaped acoustic wave front, as shown in Fig. 1(e). The spindle-shaped acoustic wave front propagates along the reverse direction until the right half of the spindle-shaped sound wave front is reflected. Then, the spindle-shaped sound wave front changes to an annular acoustic wave front again, as seen from Fig. 1(h). However, the outer sound pressure of the annular acoustic wave front is negative and the inner sound pressure is positive; specifically, the sound pressure situation of the annular acoustic wave front in Fig. 1(h) is opposite to that in Fig. 1(c). The new annular acoustic wave front finally converges in the right focus of the ellipse, as shown in Fig. 1(j). The sound pressure at the right focus in Fig. 1(j) is nearly equivalent to the sound pressure at the left focus in Fig. 1(a). The converged annular acoustic wave front acts as a new point sound source and emits an annular acoustic wave front that propagates to the right. Then, a new propagation begins. The pulse sound wave will reflect and focus back and forth between the two focus points of the ellipse. Considering that the medium is viscous and heat transfer exists between the expansion zone and compression zone in the medium, the ultrasound will attenuate and the energy of this single pulse sound wave will be reduced to zero.

From Fig. 1, it can be seen that waves can focus at the focus point, which guarantees larger ultrasonic energy around this point. It is also shown in Fig. 1 that the propagation process of the wave is stable and periodic, and thereby, the phase difference among the focused waves can be independent with time, which is necessary to interference and form a standing wave in the cavity.

The necessary conditions of interference include that the waves should have a constant phase difference, as well as the same vibration direction and frequency, when they meet at a field point. Furthermore, in order to set up a standing wave field, the waves should

also have a reverse propagating direction. In this paper, the local sound intensity is strengthened by the interference enhancement of the reflected waves and the standing wave. To guarantee a constant phase difference, the difference in the propagating distances of all the waves should not change with time when these waves meet at a field point. Hence, an elliptical cross section is ideal because the wave propagation is periodic and symmetrical along the long axis of the ellipse, based on Fig. 1. Ultrasonic wave 1 emitted from sound source F1 is reflected at point P1 and then arrives at focus point F2 where it will meet ultrasonic wave 2 reflected at P2, as shown in Fig. 2. The resultant motion of these two waves at focus point F2 is vibration along the x-axis direction. The propagating distances of these two waves are both equal to

$$S_1 = |F1P1| + |P1F2|. \tag{3}$$

At focus point F2, the resultant wave of ultrasonic wave 1 and ultrasonic wave 2 meets ultrasonic wave 4, which is emitted from sound source F1 and propagates directly along the x-axis. Ultrasonic wave 4 and the resultant wave satisfy the interference condition. To ensure that focus point F2 is a point enhanced by interference, the difference in their propagating distances should satisfy an integral multiple of the wavelength.[17] That is,

$$|F1P1| + |P1F2| - |F1F2| = k_1\lambda, \quad k_1 = 1, 2, 3, 4, 5, 6\ldots, \tag{4}$$

where λ is the wavelength, which is 55.4 mm in this paper, and k_1 is an integer.

Ultrasonic wave 1 will continue to travel from focus point F2 and is reflected at point P2 before arriving at sound source F1 again. At sound source point F1, ultrasonic wave 1 meets its reverse wave, namely, ultrasonic wave 3, which travels along the reverse path of ultrasonic wave 1. Ultrasonic wave 1 and ultrasonic wave 3 satisfy the standing wave condition. To set up the standing wave field and make the sound source an enhanced point by interference, the difference in their propagating distances should satisfy an integral multiple of wavelength.[17] That is,

$$S_2 = |F1P1| + |P1F2| + |F2P2| + |P2F1| = 2S_1 = k_2\lambda,$$
$$k_2 = 1, 2, 3, 4, 5, 6, \ldots. \tag{5}$$

In this paper, a conical transducer (28 kHz–100 W) is adopted as the sound source. A cavity with an elliptical cross section cannot provide the circular contact surface between the sound source and the cavity. Therefore, the left part of the ellipse is cut along line MN, as shown in Fig. 1.
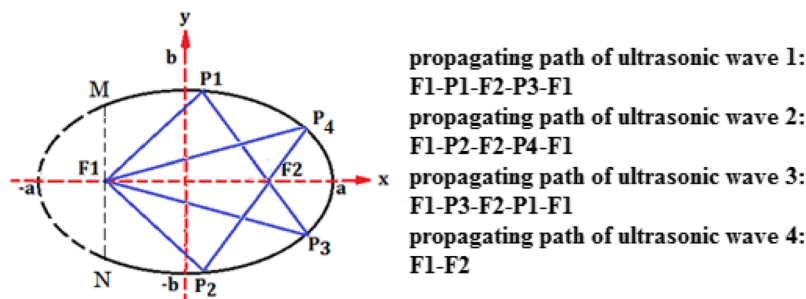

propagating path of ultrasonic wave 1:
F1-P1-F2-P3-F1
propagating path of ultrasonic wave 2:
F1-P2-F2-P4-F1
propagating path of ultrasonic wave 3:
F1-P3-F2-P1-F1
propagating path of ultrasonic wave 4:
F1-F2

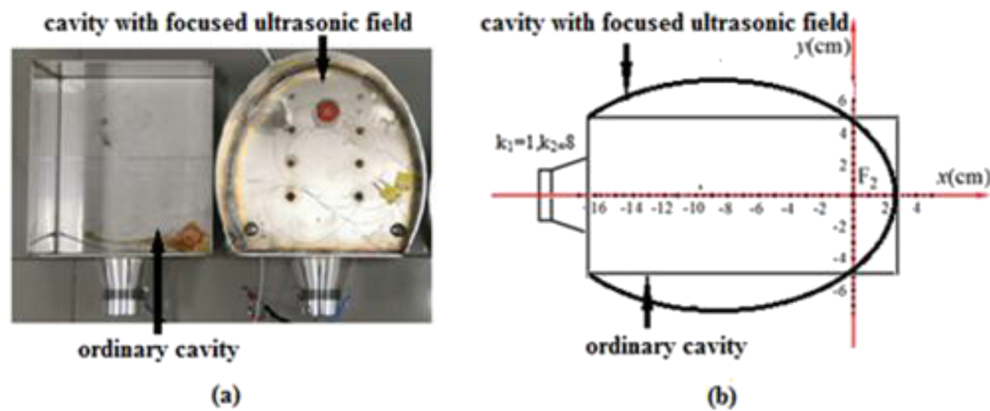**FIG. 2**. Schematic diagram of the propagating paths of the ultrasonic waves in an ellipse.

FIG. 3. The profiles of the two cavities and their relative geometric size. (a) Profiles of the cavities and (b) relative geometrical size (plane z = 50 mm).

The three-dimensional cavity with a focused ultrasonic field is obtained by stretching the two-dimensional ellipse shown in Fig. 1 along the z-axis. The ultrasonic transducer is mounted at focus point F1 on plane z = 50 mm. Figure 3(a) shows the profiles of a cavity with a focused ultrasonic field and an ordinary cavity, and Fig. 3(b) shows the relative geometric sizes of their cross sections (z = 50 mm plane). The cross section of the cavity with a focused ultrasonic field is part of an ellipse, which satisfies Eqs. (2) and (3) ($k_1 = 1$, $k_2 = 8$). The cross section of the ordinary cavity is a rectangle. The heights of these two cavities are both z = 120 mm.

III. EXPERIMENT OF ULTRASONIC HEAT TRANSFER ENHANCEMENT UNDER THE NATURAL CONVECTION REGIME

The sound intensity distributions and the heat transfer performances of the cavity with a focused ultrasonic field and an ordinary cavity (shown in Fig. 3) are tested successively. The measurement coordinate systems of the two cavities are the same as what is shown in Fig. 3(b). Figure 4 shows the experimental setup. The cavities are made of a stainless-steel plate with a thickness of 2 mm. The ultrasonic transducer driven by an ultrasonic generator (Komeida, KMD-M1) is fixed at sound source F1 (on plane z = 50 mm). The ultrasonic power and the ultrasonic frequency are 100 W and 28 kHz, respectively. The cavity is rigid, and no vibration was noted in measurements. The heat transfer copper tube or the probe of the sound intensity measuring instrument (JY-J100M, accuracy 0.01 W cm^{-2}) is connected to a fixed cross bracket, which can enable the heat transfer copper tube or the probe (stainless steel, length 40 cm, p–p style, calibrated by using a calibrator provided by the supplier) to move along the x-axis and y-axis on the measuring plane (z = 50 mm plane). The x-axis and y-axis coordinates of the copper tube or the probe are marked by the scale inscribed on the cross bracket. A single-end heating rod is inserted into the copper tube as the heat source. The contact surface between the single-end heating rod and the copper tube is coated by silicone grease (conductivity 4.5 W m^{-1} K^{-1}) to reduce the contact thermal resistance. Ten T-type thermocouples with a diameter of 0.6 mm and 0.5 °C accuracy are attached to the outer surface of the copper tube. Four other T-type thermocouples with diameters of 1.5 mm and 1 °C accuracies are placed at different heights around the copper tube. When the temperatures reach a stable state, the temperature data are recorded
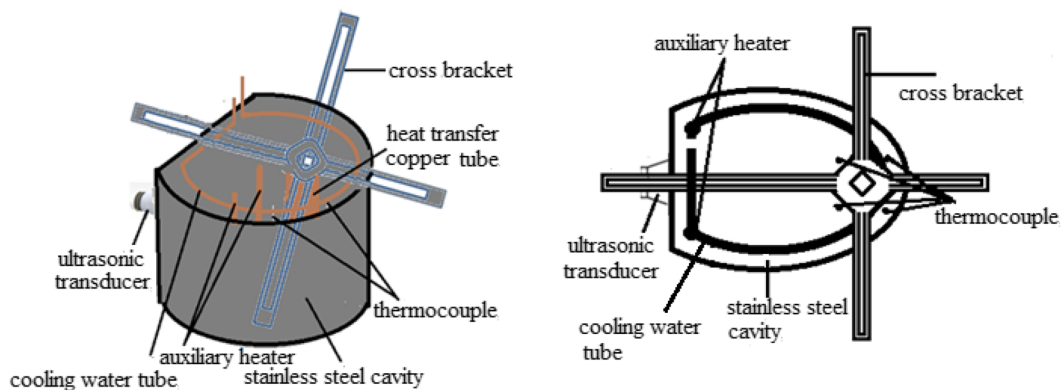

FIG. 4. The experimental setup of the sound intensity and the heat transfer performance.

by using a data acquisition system (HIOKI-LR8510). The arithmetic average value of the temperatures collected by using the ten thermocouples is taken as the wall temperature of the heat transfer copper tube, and the arithmetic average value of the four thermocouples is taken as the water temperature. Two auxiliary heaters are installed at the two corners of the cavity to keep the water temperature constant. The heating powers of the single-end heating rod and the auxiliary heaters are adjusted by using transformers and are, respectively, measured by using power meters.

Deionized water is poured into the cavity until the liquid height is 100 mm (z = 100 mm) and is heated to boil for more than 30 min for degassing. When it is cooled to room temperature, cooling water circulation and auxiliary heaters are turned on to heat the water and maintain the water temperature at 40 °C. If the sound intensity is tested, the probe of the sound intensity measuring instrument is connected to the cross bracket instead of the heat transfer copper tube. The sound intensity is then tested every 2.5 mm along the x-axis or y-axis. When the indicator of the sound intensity measuring instrument is stable, the sound intensity is recorded and then the probe is moved to the next measuring position. To eliminate error, the sound intensity measurement experiment is repeated four times and the arithmetic average value is adopted. After the sound intensity experiments, the probe of the sound intensity measuring instrument is removed and the heat transfer copper tube is installed to the cross bracket in order to test the heat transfer performance. The heating power of the copper tube is 200 W. The temperatures are collected once per second for 3 min; then, the copper tube is moved to another test point along the cross bracket. The heat transfer copper tube is moved in the same way as the probe of the sound intensity measuring instrument. The experiments are repeated three times, and no apparent difference is detected.

The heat flux q on the surface of the heat transfer copper tubes is calculated by

$$q = \frac{P}{\pi D l}, \qquad (6)$$

where P is the heating power of the single-end heating rod and D and l are the diameter and the length of the copper tube, respectively. Therefore, heat flux q is 37 kW m^{-2} here.

The heat transfer coefficient h can be calculated by

$$h = \frac{T_{tube} - T_{water}}{q}, \qquad (7)$$

TABLE I. Uncertainty analysis.

	Tested value	Uncertainty
Measured parameter		
T_{water} (°C)	50	±1
T_{tube} (°C)	75	±0.5
l (mm)	80	<0.05
D (mm)	20	<0.05
Calculated parameter		
Surface area of the tube	5.03×10^{-3} m^2	0.17%
q	1.85×10^4 W m^{-2}	3.0%
h	1000 W m^{-2} K^{-1}	4.2%

where T_{tube} is the surface temperature of the copper tube and equals the arithmetic average value of the ten thermocouples. T_{water} is the temperature of the water and equals the arithmetic average value of the four thermocouples.

The accuracies of the length and the temperature measurements are listed in Table I. Therefore, according to Ref. 18, the uncertainties in the surface area of the copper tube and heat flux are 0.17% and 3%, respectively. The maximum error for the heat transfer coefficient is 4.2%.

IV. RESULTS AND DISCUSSION

Because the instantaneous sound pressure will change positively and negatively with time, the sound intensity probe measures time-averaged sound intensity only. Figure 5 shows the sound intensity distributions along the x-axis (y = 0 mm, z = 50 mm) and the y-axis (x = 0 mm, z = 50 mm) in the cavity with a focused ultrasonic field and the ordinary cavity. From Fig. 5, it can be determined that the maximum sound intensity is located near the focus point F2 (x = 0 mm, y = 0 mm, and z = 50 mm) in the cavity with a
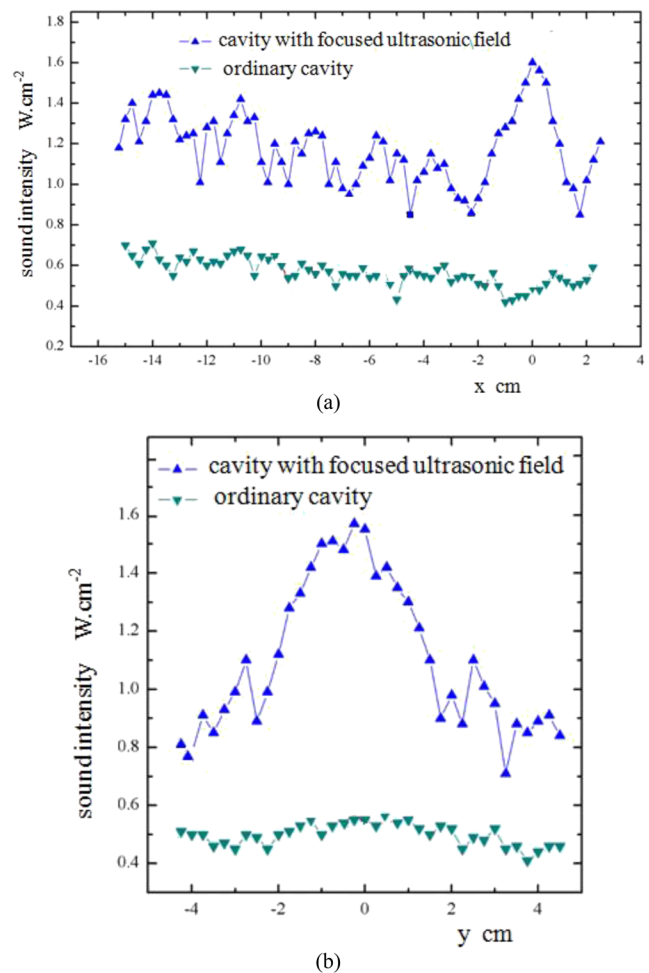

(a)

(b)

FIG. 5. The sound intensity along the x-axis and y-axis: (a) x-axis and (b) y-axis.

focused ultrasonic field and has a value of 1.56 W cm^{-2}. Five smaller peaks of sound intensity appear between sound source F1 and focus point F2 along the x-axis in the cavity with a focused ultrasonic field. This result is consistent with the standing wave characteristic, considering that the distance F1F2 is three times that of the wavelength. Whether it is along the x-axis or along the y-axis, the sound intensity in the cavity with a focused ultrasonic field displays a wavy pattern and is always larger than that in the ordinary cavity. The patterns of the sound intensity along both the x-axis and y-axis in the ordinary cavity look gentler.

Figure 6 gives the heat transfer coefficients along the x-axis (y = 0 mm, z = 50 mm) and the y-axis (x = 0 mm, z = 50 mm) in the cavity with a focused ultrasonic field and the ordinary cavity. It can be determined from Fig. 6 that the maximum heat transfer coefficient appears at the focus point in the cavity with a focused ultrasonic field and has a value of 1574.3 W m^{-2} K^{-1}. There are also five smaller peaks along the x-axis in the cavity with a focused ultrasonic field. The coordinates of the peaks of the heat transfer coefficient are quite close to the coordinates of the peaks of the sound intensity when comparing Figs. 5 and 6. The heat transfer coefficients in the ordinary cavity along both the x-axis and y-axis are uniform and are smaller than those in the cavity with a focused ultrasonic field.
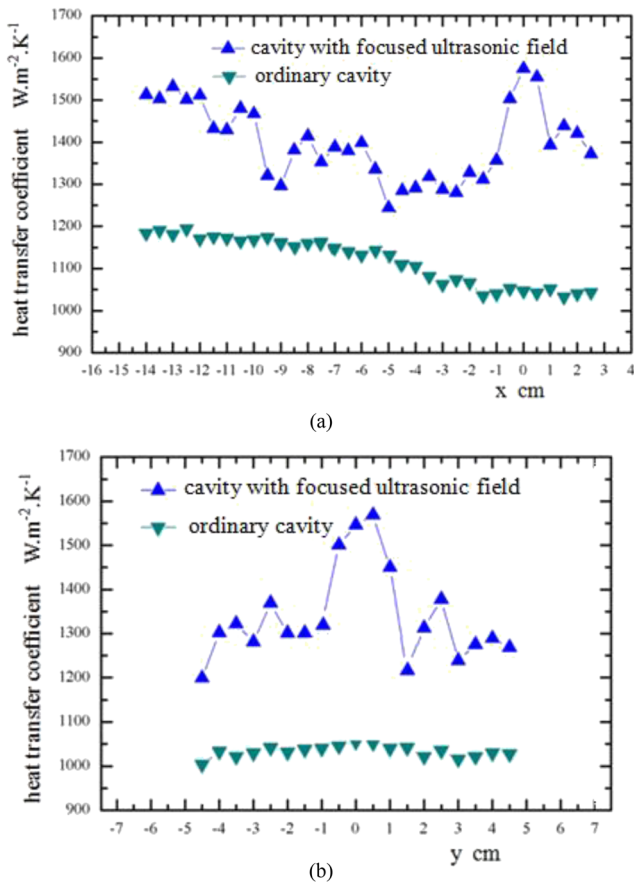

(a)

(b)

FIG. 6. The heat transfer coefficient along the x-axis and y-axis: (a) x-axis and (b) y-axis.

Therefore, it can be concluded that, at focus point F2 in the cavity with a focused ultrasonic field, the sound intensity is enhanced by interference as well as the standing wave, and as a result, the heat transfer is improved by the enhanced sound intensity.

Ultrasonic cavitations and acoustic streaming, which all depend on the sound intensity near the heat transfer interface, are responsible for the ultrasonic heat transfer enhancement. Acoustic streaming is produced by the viscosity of the working fluid and can disturb the working fluid, thin the thermal boundary layer, and enhance convection. The stronger the sound intensity is, the larger the velocity of the acoustic streaming is. In this paper, the acoustic streaming characteristics in the cavity with a focused ultrasonic field and the ordinary cavity are observed and compared.

The thermoacoustic field can be represented by the first and the second order of the acoustic perturbation in temperature T, pressure p, and velocity $\vec{v}$,[19]

$$T = T_0 + T_1 + T_2, \tag{8}$$

$$p = p_0 + p_1 + p_2, \tag{9}$$

$$\vec{v} = \vec{v}_1 + \vec{v}_2. \tag{10}$$

The subscripts 0, 1, and 2 denote the cases without acoustic perturbation, the first order, and the second order, respectively. The fluid is at the equilibrium state and is quiescent before the first order acoustic perturbation is added. To the first order of the ultrasonic field,[19] the governing equations are

$$\frac{\partial T_1}{\partial t} = D_{\text{th}} \nabla^2 T_1 + \frac{\alpha T_0}{\rho_0 C_p} \frac{\partial p_1}{\partial t}, \tag{11}$$

$$\frac{\partial p_1}{\partial t} = \frac{C_v}{C_p \cdot \kappa} \left(\alpha \cdot \frac{\partial T_1}{\partial t} - \nabla \cdot \vec{v}_1 \right), \tag{12}$$

$$\rho_0 \frac{\partial \vec{v}_1}{\partial t} = -\nabla p_1 + \eta \nabla^2 \vec{v}_1 + \beta \eta \nabla (\nabla \cdot \vec{v}_1), \tag{13}$$

$$\alpha = -\frac{1}{\rho} \left(\frac{\partial \rho}{\partial T} \right)_p, \tag{14}$$

$$\kappa = \frac{1}{\rho} \left(\frac{\partial \rho}{\partial p} \right)_s. \tag{15}$$

Here, D_{th} is the thermal diffusivity, η is the dynamic viscosity, and β is the viscosity ratio and is 1/3 for a simple liquid. α and κ are the isobaric thermal expansion coefficient and the isentropic compressibility, respectively. The boundary conditions on the first order variables are

$$\frac{\partial p_1}{\partial \vec{n}} = 0 \text{ on all walls,} \tag{16}$$

$\vec{v}_1 = v_m e^{-i\omega t} \vec{e}_r$ added ultrasound at point F1 with coordinates

$$\times (166.2 \, \text{mm}, 0.50 \, \text{mm}), \tag{17}$$

$$T_{1\infty} = 40\,^\circ\text{C}, \quad -k'_T \nabla \cdot T_1 = q \text{ (heat source)}. \tag{18}$$

Equation (16) means that there is no-slip between the wall and the fluid. Equation (17) presents the external ultrasound actuation

having harmonic time dependence. $\vec{n}$ is the normal unit vector. v_m is the amplitude of the velocity, and ω is the angular frequency. $\vec{e}_r$ is the outward unit vector along the wave vector direction. κ'_T is the thermal conductivity of the medium. $T_{1\infty}$ is the temperature of the bulk fluid.

For water and most other liquids, the coupling of the temperature field T_2 with the variables $\vec{v}_2$ and p_2 in the second order governing equations can be neglected.[19] Considering the first order field is harmonic time dependent inherited from the perturbation at point F1 [Eq. (17)], the time average over a full oscillation period (represented by brackets $\langle\cdots\rangle$) of the second order governing equations becomes

$$\rho_0 \nabla \cdot \langle \vec{v}_2 \rangle = -\nabla \cdot \langle \rho_1 \vec{v}_1 \rangle, \quad (19)$$

$$\eta \nabla^2 \langle \vec{v}_2 \rangle + \beta\eta \nabla(\nabla \cdot \langle \vec{v}_2 \rangle) - \langle \nabla p_2 \rangle = \rho_0 \langle (\vec{v}_1 \cdot \nabla)\vec{v}_1 \rangle + \left\langle \rho_1 \frac{\partial \vec{v}_1}{\partial t} \right\rangle. \quad (20)$$

From Eqs. (19) and (20), it can be seen that the products of the first order field are the source terms for the second order field. Because of the harmonic time dependence of the first field, the second order fields of $\vec{v}_2$ and p_2 are nonzero in the viscous medium. In theory, by solving the second order field, the acoustic streaming feature can be obtained.

In this paper, the methylene blue aqueous solution (15 ml) is injected slowly into either the sound source point or the focus point F2 (x = 0 mm, y = 0 mm, z = 50 mm) of the cavity by using a microsyringe to observe acoustic streaming in the cavities. Then, the motion of the methylene blue solution is captured by using a camera. The flow of the methylene blue solution in the cavity is under the influence of the ultrasound field and can qualitatively represent the situation of acoustic streaming. Figure 7 shows the diffusions of the methylene blue solution injected at the sound source point and the focus point in the cavity with a focused ultrasonic field. When the methylene blue solution is injected at the sound source point, it first flows rapidly toward the focus point along the x-axis with a jet-like pattern because the sound intensity in the standing wave field is stable and symmetrical to the x-axis in the cavity with a focused ultrasonic field. Then, the methylene blue solution begins to diffuse into a mushroom cloud pattern and finally disappears gradually. The position where the methylene blue solution begins to diffuse is about half a wavelength away from the source point because the phase difference between the two adjacent nodes in the standing wave field imposes an influence on the acoustic streaming and boosts the diffusion of the methylene blue solution.

When the methylene blue solution is injected at the focus point in the cavity with a focused ultrasonic field, it has a smaller initial flow velocity along the x-axis than when it is injected at a sound source point. The methylene blue solution does not go far away from the focus point along the x-axis, and it subsequently begins to slowly spread out of the focus point with a flocculent pattern. This is because the focus point is near the cavity wall, and as a result, the acoustic streaming line should be closed there. The pattern of diffusion of the methylene blue solution around the focus point means that acoustic streaming around the focus point is helpful for transferring heat to the surrounding area.
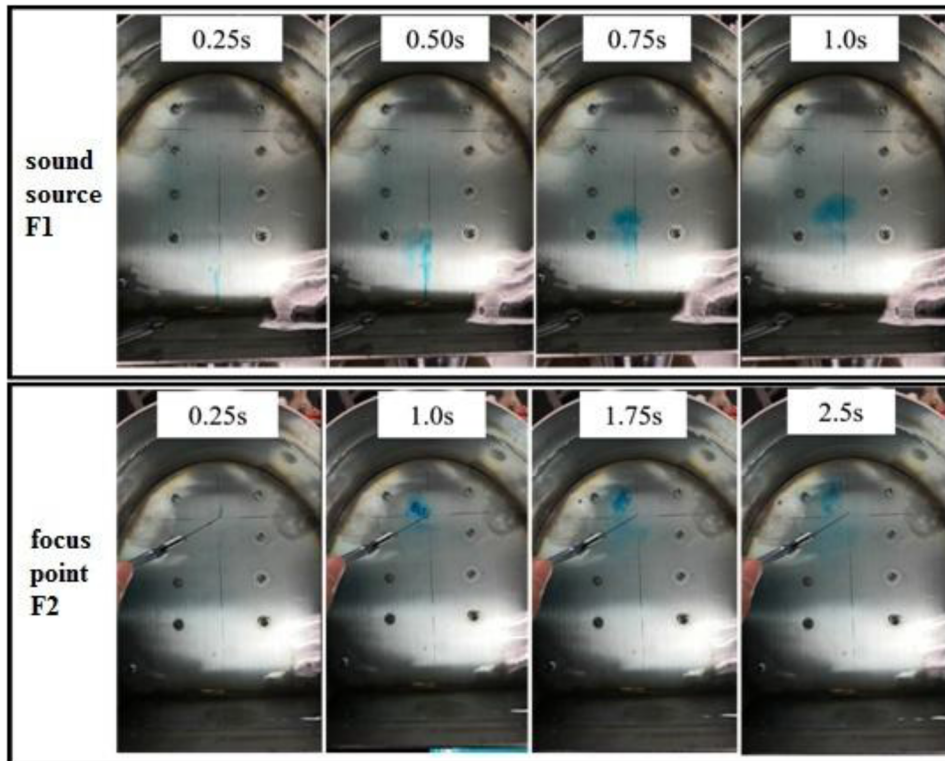

FIG. 7. Diffusion of the methylene blue solution in the cavity with a focused ultrasonic field.
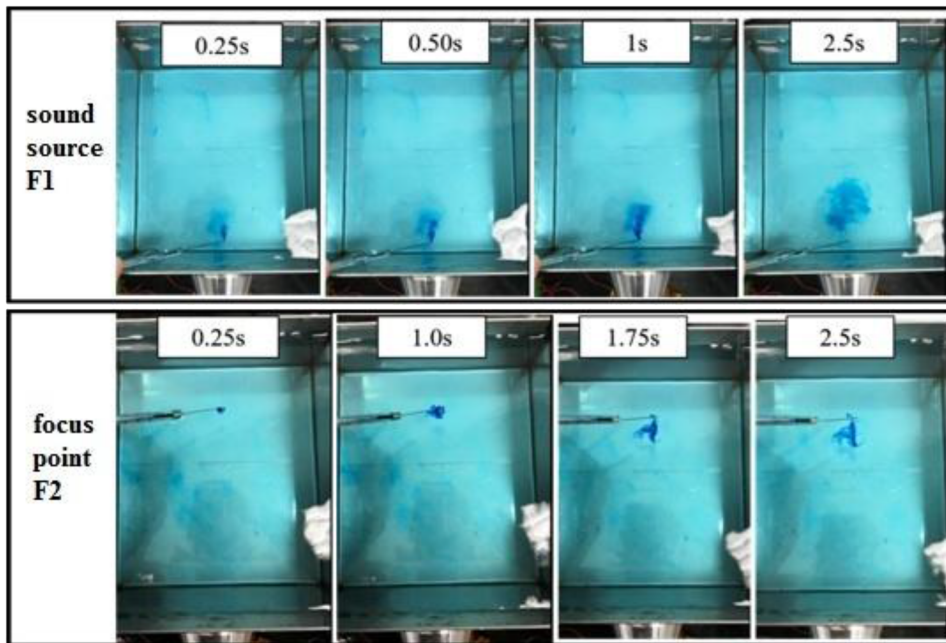
FIG. 8. Diffusion of the methylene blue solution in the ordinary cavity.

Figure 8 shows the diffusions of the methylene blue solution injected at the sound source point and at the focus point in the ordinary cavity. From Fig. 8, it can be seen that when the methylene blue solution is injected at the sound source, it first flows toward the focus point along the x-axis. However, the flow distance of the methylene blue solution in the ordinary cavity at 0.25 s is only half of that in the cavity with a focused ultrasonic field comparing Figs. 7 and 8. This means that, because sound intensity along the x-axis in the ordinary cavity is weaker than that in the cavity with a focused ultrasonic field, the acoustic streaming velocity in the ordinary cavity is also lower than that in the cavity with a focused ultrasonic field. Then, the methylene blue solution diffuses outward in a fan-shaped
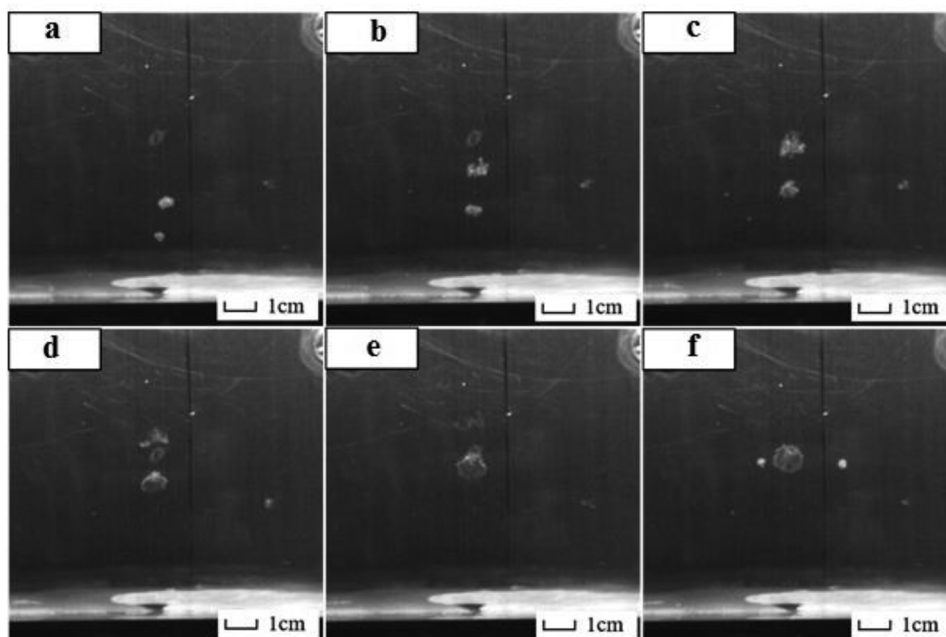

FIG. 9. Ultrasonic cavitations at the sound source: (a) time = 1570 s; (b) time = 1590 s; (c) time = 1610 s; (d) time = 1640 s; (e) time = 1670 s; and (f) time = 1690 s.
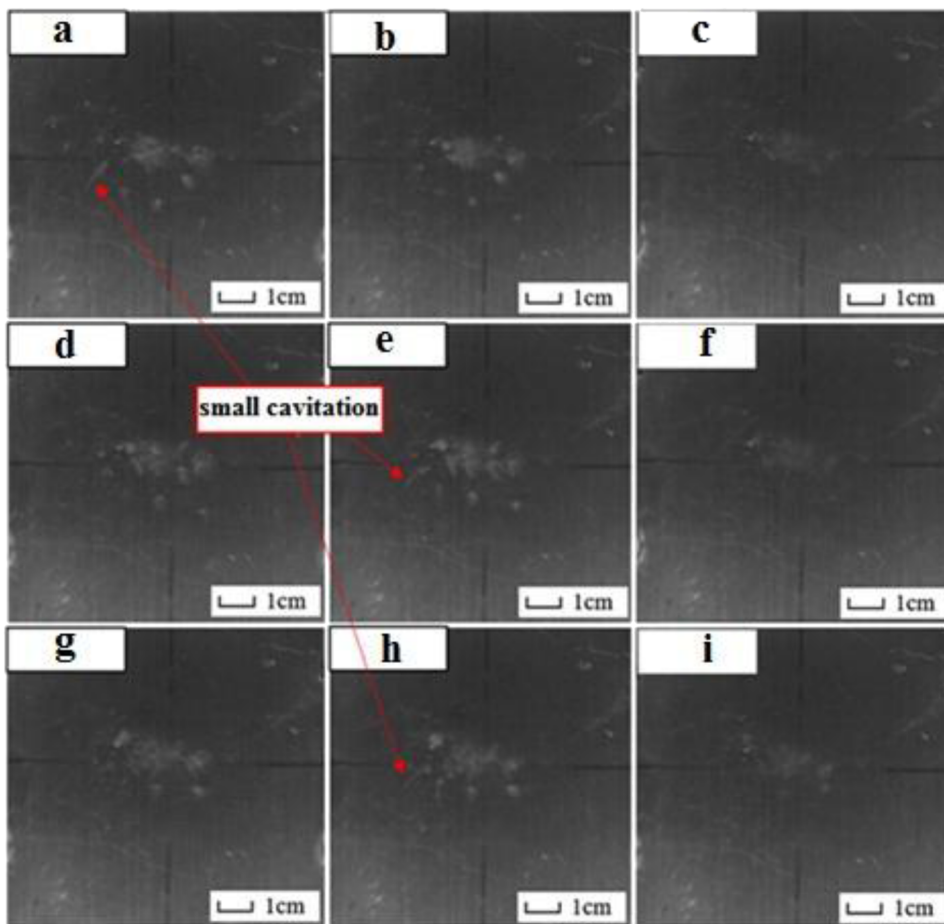
FIG. 10. Ultrasonic cavitations at the focus point: (a) time = 2440 s; (b) time = 2443 s; (c) time = 2446 s; (d) time = 2449 s; (e) time = 2451 s; (f) time = 2454 s; (g) time = 2458 s; (h) time = 2461 s; and (i) time = 2464 s.

pattern due to the unstable ultrasonic field in the ordinary cavity. The diffusion velocity in the ordinary cavity is still slower than that in the cavity with a focused ultrasonic field.

When the methylene blue solution is injected at the focus point in the ordinary cavity, it is at first nearly stationary and then begins to diffuse at 1.0 s with a velocity similar to that without an ultrasonic wave. Therefore, the velocity of acoustic streaming near the sound source in the ordinary cavity is smaller than that in the cavity with a focused ultrasonic field, and there is almost no acoustic streaming at the focus point in the ordinary cavity.

In the ordinary cavity, no ultrasonic cavitations are observed, while in the cavity with a focused ultrasonic field, ultrasonic cavitations can be observed at the focus point and the sound source. Cavitations in the cavity with a focused ultrasonic field are captured by using a high-speed camera (the number of frames taken is 1000 frames per second) and are shown in Figs. 9 and 10. It can be seen from Fig. 9 that cavitations near that sound source move toward the focus point along the x-axis under the action of acoustic streaming near the sound source. These cavitations grow and finally disappear before they arrive at the focus point.

Cavitations near the focus point gather and form a cavitation cloud under the combined action of acoustic streaming and the Bjerknes force,[20] as shown in Figs. 10(a) and 10(b). Then, the cavitations collapse, and the high temperature, higher pressure, and mic-jet effects drive and break the cavitation cloud in a short time, as shown in Fig. 10(c). The broken cavitations will become a nucleus, and new cavitations will grow and form a cavitation cloud again [see Figs. 10(d) and 10(e)]. Then, the cavitations collapse again, as shown in Fig. 10(f). Although a cavitation cloud forms a gas layer with a large thermal resistance, which is unfavorable for heat transfer, the collapse of the cavitations and the resulting high temperature, higher pressure, and mic-jet effects still contribute substantially to heat transfer, as the disturbance of the fluid around the focus point is strengthened.

V. CONCLUSION

In this paper, a focused ultrasound field was proposed with the aim of improving the ultrasonic heat transfer enhancement. The main conclusions are as follows:

(1) Whether along the x-axis or along the y-axis, the sound intensity and heat transfer coefficient in the cavity with a focused ultrasonic field display wavy patterns and are always larger than those in the ordinary cavity.

(2) The velocity of the acoustic streaming in the cavity with a focused ultrasonic field is larger than that in the ordinary cavity. The larger acoustic streaming in the cavity with a focused ultrasonic field contributes to the larger heat transfer coefficient.

(3) No cavitations are observed in the ordinary cavity. Although the cavitation cloud forms a gas layer around the focus point in the cavity with a focused ultrasonic field and is unfavorable for heat transfer, the cavitations collapse and the resulting high temperature, higher pressure, and microjet effects still contribute substantially to heat transfer.

A separate numerical modeling that takes full physics into account is worth investigating, which is expected to provide further insights into this topic.

ACKNOWLEDGMENTS

DATA AVAILABILITY

The data that support the findings of this study are available from the corresponding author upon reasonable request.

REFERENCES

[1]R. Lemlich and C.-K. Hwu, "The effect of acoustic vibration on forced convective heat transfer," AIChE J. **7**, 102–106 (1961).

[2]R. M. Fand and P. Cheng, "The influence of sound on heat transfer from a cylinder in cross flow," Int. J. Heat Mass Transfer **6**(7), 571–596 (1963).

[3]K. W. Li and J. D. Parker, "Acoustical effects on free convective heat transfer from a horizontal wire," J. Heat Transfer **89**(3), 277–278 (1967).

[4]H. K. Tam, L. M. Tam, A. J. Ghajar, and I. P. Chen, "Experimental study of the ultrasonic effect on heat transfer inside a horizontal mini-tube in the laminar region," Appl. Therm. Eng. **114**, 1300–1308 (2017).

[5]S.-W. Chen, F.-C. Liu, H.-J. Lin, P.-S. Ruan, Y.-T. Su, Y.-C. Weng, J.-R. Wang, J.-D. Lee, and W.-K. Lin, "Experimental test and empirical correlation development for heat transfer enhancement under ultrasonic vibration," Appl. Therm. Eng. **143**, 639–649 (2018).

[6]F. Baffigi and C. Bartoli, "Effects of ultrasounds on the heat transfer enhancement from a circular cylinder to distilled water in subcooled boiling," J. Therm. Sci. Eng. Appl. **3**(1), 011001 (2011).

[7]B. Liu, J. Cai, and X. Huai, "Heat transfer with the growth and collapse of cavitation bubble between two parallel heated walls," Int. J. Heat Mass Transfer **78**, 830–838 (2014).

[8]S.-V. Orandrou, J.-C. Roy, Y. Bailly et al., "Determination of the heat transfer coefficients for the combined natural and streaming convection on an ultrasonic transducer," Int. J. Heat Mass Transfer **62**(4), 402–410 (2013).

[9]M. Zheng, B. Li, Z. Wan et al., "Ultrasonic heat transfer enhancement on different structural tubes in LiBr solution," Appl. Therm. Eng. **106**(Suppl. C), 625–633 (2016).

[10]F. Baffigi and C. Bartoli, "Influence of the ultrasounds on the heat transfer in single phase free convection and in saturated pool boiling," Exp. Therm. Fluid Sci. **36**(Suppl. C), 12–21 (2012).

[11]N. Zhao, B. Fu, and H. B. Ma, "Ultrasonic effect on the bubble nucleation and heat transfer of oscillating nanofluid," Appl. Phys. Lett. **104**, 263105 (2014).

[12]R. Mathur, G. Aggarwal, B. Satsangi et al., "Experimental study on the effects of acoustic streaming of high frequency ultrasonic waves on convective heat transfer: Effects of transducer position and wave interference," Int. Commun. Heat Mass Transfer **39**(5), 720–725 (2012).

[13]C. Bartoli and F. Baffigi, "Effects of ultrasonic waves on the heat transfer enhancement in subcooled boiling," Exp. Therm. Fluid Sci. **35**(3), 423–432 (2011).

[14]J.-P. Xia and H.-X. Sun, "Acoustic focusing by metal circular ring structure," Appl. Phys. Lett. **106**(6), 063505 (2015).

[15]J.-p. Xia, H.-x. Sun, Q. Cheng, Z. Xu, H. Chen, S.-q. Yuan, S.-y. Zhang, Y. Ge, and Y.-j. Guan, Appl. Phys. Express **9**, 057301 (2016).

[16]K. Hong and J. Kim, "Natural mode analysis of hollow and annular elliptical cylindrical cavities," J. Sound Vib. **183**(2), 327–351 (1995).

[17]G. Du, Z. Zhu, and X. Gong, Basic Theory of Acoustics (Nanjing University Press, Nan Jing, 2018), pp. 147–152.

[18]R. J. Moffat, "Describing the uncertainties in experimental results," Exp. Therm. Fluid Sci. **1**(1), 3–17 (1988).

[19]P. B. Muller, R. Barnkob, M. J. H. Jensen, and H. Bruus, "A numerical study of microparticle acoustophoresis driven by acoustic radiation forces and streaming-induced drag forces," Lab Chip **12**, 4617–4627 (2012).

[20]Z. Douglas, T. R. Boziuk, M. K. Smith, and A. Glezer, "Acoustically enhanced boiling heat transfer," Phys. Fluids **24**, 052105 (2012).